REVIEW

Metal oxide and hydroxide nanoarrays: Hydrothermal synthesis and applications as supercapacitors and nanocatalysts

Qiu Yang, Zhiyi Lu, Junfeng Liu*, Xiaodong Lei, Zheng Chang, Liang Luo, Xiaoming Sun*

State Key Laboratory of Chemical Resource Engineering, Beijing University of Chemical Technology, Beijing 100029, China

Abstract   The development of nanotechnology in recent decades has brought new opportunities in the exploration of new materials for solving the issues of fossil fuel consumption and environment pollution. Materials with nano-array architecture are emerging as the key due to their structure advantages, which offer the possibility to fabricate high-performance electrochemical electrodes and catalysts for both energy storage and efficient use of energy. The main challenges in this field remain as rational structure design and corresponding controllable synthesis. This article reviews recent progress in our laboratory related to the hydrothermal synthesis of metal oxide and hydroxide nanoarrays, whose structures are designed aiming to the application on supercapacitors and catalysts. The strategies for developing advanced materials of metal oxide and hydroxide nanoarrays, including NiO, Ni(OH)$_2$, Co$_3$O$_4$, Co$_3$O$_4$@Ni–Co–O, cobalt carbonate hydroxide array, and mixed metal oxide arrays like Co$_{3-x}$Fe$_x$O$_4$ and Zn$_x$Co$_{3-x}$O$_4$, are discussed. The different kinds of structure designs such as 1D nanorod, 2D nanowall and hierarchical arrays were involved to meet the needs of the high performance materials. Finally, the future trends and perspectives in the development of advanced nanoarrays materials are highlighted.

*Corresponding authors. Tel.: +86 10 64448751; fax: +86 10 64425385.

E-mail addresses: ljf@mail.buct.edu.cn (J. Liu), sunxm@mail.buct.edu.cn (X. Sun).

Production and hosting by Elsevier

1. Introduction

One-dimensional (1D) or two-dimensional (2D) nanostructures such as nanowires, nanotubes, nanoribbons and nanosheets are continuing to be at the forefront of nanoscience and nanotechnology due to their unique chemical and physical properties, which can be attributed to their dimensional anisotropy [1–5]. They are arguably the most studied nanomaterial model to fabricate functional devices and have been demonstrated to be the optimized architecture for electronic/electrochemical electrodes, especially, when they are applied in the form of oriented arrays [6,7]. The versatile utilization of energy in an efficient and clean way has received worldwide concern and increased research interest. Energy storage becomes even more complex and important by converting one type of energy into another form of energy that can be stored and converted for use when needed aiming at proper utilization of different energy sources. The application of catalysts also plays an important role in energy and environment areas that are closely related to the humankind. The improvement of their overall performance, mainly including the activity and stability, significantly depends on the advancement of new materials used in these processes, especially in a large part of "how to design superior architectures".

It is generally accepted that the surface (or interface) reactions are critical in many processes, from electrochemical processes on an electrode to heterogeneous catalytic reactions [8–10]. Therefore, researchers prefer to synthesize nanomaterials with smaller size to ensure that larger surfaces are exposed. However, the traditional nanoparticles often become unstable and tend to diminish during the reactions when the size is reduced to an extreme small value. The aggregation of active materials of electrochemical electrodes or catalysts tends to reduce the accessible surface area for participating reactions, resulting in a decrease in their activities. One of the ways to address these issues is to construct ordered architectures by having 1D or 2D nanostructures grown in a vertical fashion forming geometrically confined structures, instead of traditional nanoparticles [11–13]. Nanoarrays, with their 1D/2D morphologies, e.g. their length at microscale and their diameter/thickness dimensions at nanoscale, often exhibit fascinating properties, such as larger surface area, uniform structure and high porosity architectures [14–16]. These properties are highly desired for supercapacitor electrode, because it could prevent agglomeration, facilitate the electron transfer rate and the penetration of the electrolytes into the whole electrode matrix [8,17,18], as well meet the needs of the development trend of catalysis in the structured way, providing more active sites and making the catalyst more stable [19,20]. However, these potentials highly rely on the subtle control of their physical properties such as their density of active site and the transport of electrons and reactants. These can be tailored over a wide range of material parameters like compositions, size and three-dimensional morphology, which make these nanoarrays so outstanding and intensively researched. Over the last few decades, 1D or 2D nanoarrays that have been mainly in the research focus in these respects include carbon nanotubes (CNTs), metal oxide nanotubes and nanowires (e.g. ZnO, TiO$_2$, V$_2$O$_5$, Cu$_2$O, NiO, Fe$_2$O$_3$), silicon nanowires, as well as III–V or II–VI based hetero-nanostructures, metallic nanowires and hybrid of structures of multiple compositions [6,7,21–31]. For example, Cui's group reported a Si nanowire arrays (NWAs) anode which was grown directly on the metallic current collector substrate can improve the rate capability and stability significantly [32]. Li et al. used a template-free growth method to prepare Ni$_x$Co$_{3-x}$O$_4$ nanowire arrays electrode that showed high catalytic activity for OER with optimized Ni:Co ratio [33].

In general, the key factors for nanostructured arrays or higher level nanoarchitectures as advanced electrochemical electrodes or structured catalysts are: (1) large active surface area; (2) high electric or thermal conductivity of the active material; and (3) excellent connection and contact between active materials and substrates. Hence, the rational design and controllable synthesis of the nanoarrays are required. Commonly, there are two different kinds of methods that have been developed for the chemical preparation of nanoarrays. One is dry routes such as the atmospheric pressure chemical vapor deposition (APCVD) approach [34,35], and another is wet routes including various solution-based chemical strategies [36], which is considered much more flexible for nanocrystal synthesis [37].

In this review, we provide a brief account of our recent efforts to synthesize nanoarrays using hydrothermal methods. A special emphasis is laid on the research aiming at designing advanced materials for supercapacitor and catalytic applications. Transition metal oxides and hydroxide were chosen, because they have multiple oxidation states that enable rich redox reactions for pseudocapacitance generation and catalytic reactions. By utilizing simple hydrothermal reactions and controlling reaction parameters (concentration, reaction temperature, reaction time, etc.), we have obtained different kinds of nanoarray structures (nanorod, nanowall, hierarchical nanosheet@nanowire, ultrathin nanosheet, etc.) of various materials (metals oxides, metal hydroxide, mixed metals oxide, etc.). Subsequently, we focus on the supercapacitor and catalytic applications of nanoarrays and summarize our recent endeavors in the study of nanoarray electrode materials and nanocatalysts. In the last part, an outlook on this field of research will be given as well.

2. Hydrothermal synthesis of metal oxide and hydroxide nanoarrays

The controllable fabrication of highly ordered nanostructure on substrate has been widely studied by using kinds of methods, such as high-temperature vapor-phase approaches including physical vapor deposition and chemical vapor deposition [38–40], and low-temperature solution-based chemical strategies including hydrothermal method, electrochemical synthesis method and the sol gel method [14,41–43]. Compared with vapor-phase approaches, which are expensive and energy-consuming, solution-based synthetic strategies have the advantages of saving energy, convenient manipulation, excellent control over size and morphology, and greater capability and flexibility. Among them, hydrothermal synthetic strategies on a water system are considered as simple and powerful routes and become more popular in fabricating ordered nanoarray structures recently. This method relies on the chemical reactions and solubility changes of substances in a sealed heated aqueous solution above ambient temperature and pressure to grow nanocrystals. Recently, Zhang et al. introduced several types of representative hydrothermal synthetic strategies of inorganic semiconducting nanostructures in detail [44]. They pointed out that precise control over the hydrothermal synthetic conditions is a key to the success of the preparation of high-quality inorganic semiconducting nanostructures. Therefore, for the purpose of building nanostructure arrays with satisfactory morphology,

controlling the reaction conditions and designing the reaction processes are critical.

In this section, we will introduce several novel hydrothermal strategies involved in our previous works for synthesizing various nanoarray structures, such as 1D nanorod, 2D nanowall and hierarchical arrays. Besides single phase materials (NiO, Ni(OH)$_2$, Co$_3$O$_4$), composite materials containing multiple metal ions (Co$_3$O$_4$@Ni–Co–O, Co$_{3-x}$Fe$_x$O$_4$, Zn$_x$Co$_{3-x}$O$_4$) are also developed to achieve the synergy effect of the different components and enhance the scope of functionality further. All the reactions occurred in Teflon-lined stainless-steel autoclaves and the reaction temperature distributes in a low range (100–120 °C), which can provide a stable high-pressure environment for the reaction and make the synthetic strategies more safety and economical.

2.1.   1D or 2D nanoarray

1D or 2D nanoarrays like NiO nanorod, Ni(OH)$_2$ nanowall and Co$_3$O$_4$ nanowire/nanosheet arrays can be achieved via simple hydrothermal method of directly putting the substrates into corresponding reaction solutions (contain metal salts and alkali), maintaining for a certain time at appropriate temperature and following annealing treatment (Fig. 1). The morphology and size of these nanoarrays mainly depend on the reaction conditions, such as reaction temperature, reaction time, and concentration and ratios of the reactants. Briefly, the preparation of NiO nanorod (typically micrometers in length and 10–15 nm in diameter) array involved precipitation of nickel hydroxide carbonate precursor on nickel foam in aqueous solution, which is induced by urea hydrolysis upon hydrothermal treatment at 100 °C for 12 h and then conversion of the precursor to NiO by annealing in Ar at 573 K (Fig. 1a) [45]. It was interesting that when we replaced the urea with HMT

(hexamethylenetetramine), ultrathin Ni(OH)$_2$ nanowall array consisted of many sheets (typically 1 μm in length and 6 nm in thickness) could be obtained under the same reaction condition (Fig. 1b) [46]. That means the alkali has a great influence on the morphology of nanoarrays. Furthermore, Co$_3$O$_4$ nanoarrays with different morphology were also prepared by the same methodology (Figs. 1c, d) [47]. The Co$_3$O$_4$ nanosheets, which obtained by reacting cobalt salt with urea and NH$_4$F at 100 °C for 6 h and following annealing treatment, were quite uniform with the average edge and thickness size of about 6 μm and 100 nm, respectively. In another case, uniform Co$_3$O$_4$ nanowire (5–7 μm in length, 50 nm in diameter) could be achieved by increasing the reaction temperature to 120 °C and reaction time to 12 h. All the nanoarrays had strong interaction with the substrate, which was proven by the fact that even several hours of ultrasonication did not dislodge the color from the substrate. In all, this simple and easy-control hydrothermal method will be suitable for synthesizing other various 1D or 2D metal oxide nanoarray.

2.2.   Hierarchical nanoarrays

Since the structure of materials plays an important role on the performance of electrodes or catalysts, many efforts have been devoted into the design and synthesis of materials with superior architectures [11,18,23,28,48–52]. The growth and alignment of hierarchical nanoarrays based on 1D or 2D nanostructures has allowed bridging the gap from the nano into the micro- and macroworld and is essential for a variety of engineering applications. Generally, the synthetic strategy of hierarchical nanoarrays can be classified into two kinds: one-step self-template growth and multi-step-graded growth method. One-step self-template growth approach is facile and effective to some kind of hierarchical nanoarrays. It usually utilizes the main units of 1D or 2D
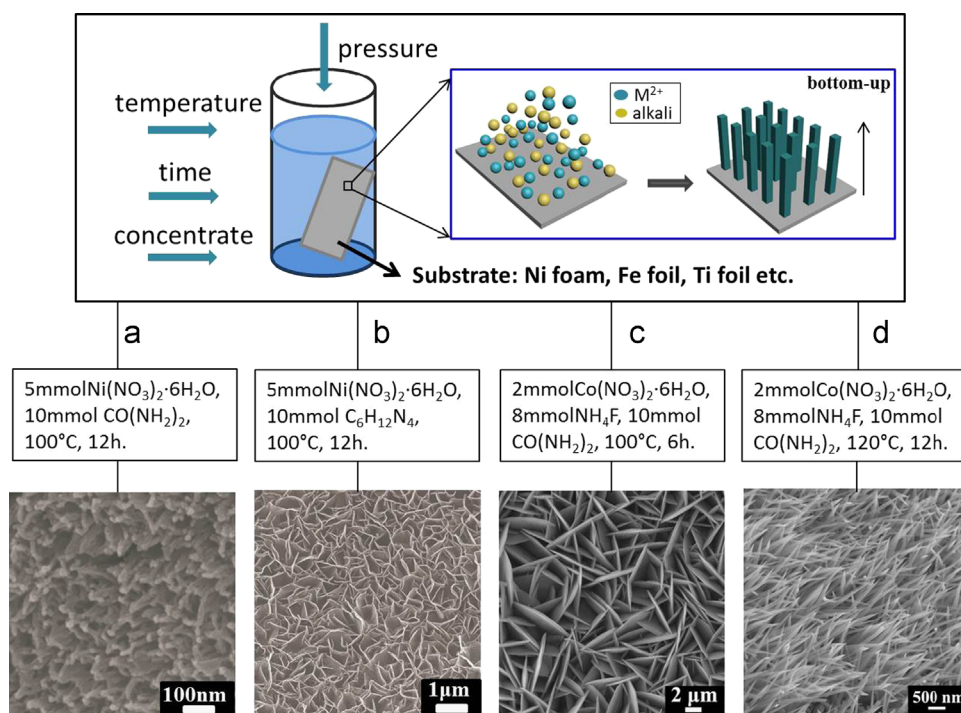
Fig. 1   Schematic diagram of hydrothermal synthesis of 1D and 2D nanoarrays. (a) NiO nanorod; (b) Ni(OH)$_2$ nanowall; (c) Co$_3$O$_4$ nanosheet; and (d) Co$_3$O$_4$ nanowire.

nanostructure as template for epitaxial growth of secondary structures via controlling the reaction condition in one pot to fabricate hierarchical structure.

Here we take hierarchical $Co_{3-x}Fe_xO_4$ arrays as an example to demonstrate this one-step self-template growth method [19]. Fig. 2 shows the schematic diagram and typical SEM images of the transformation process of hierarchical $Co_{3-x}Fe_xO_4$ arrays, which were prepared on the iron substrate by one-step hydrothermal reaction of Co^{2+} and F^- ions and urea at 120 °C for 12 h and following annealing treatment. Hexagonal cobalt iron layered double hydroxide (CoFe-LDH) platelets about 50 μm in edge length and approximately 1 μm in thickness oriented perpendicular to the surface were firstly grown on the iron substrate by hydrothermal reaction of Co^{2+} and F^- ions and urea at 120 °C for 3 h (Figs. 2b, e). Continued reaction resulted in the formation of a secondary nanostructure of iron-doped orthorhombic cobalt hydroxide carbonate (CoFe-HC) nanowires grew epitaxially out from the edges of the hexagonal CoFe-LDH platelets in a parallel fashion (Figs. 2c, f), with a length of about 4 μm and average width at the base of about 500 nm. These hierarchical structures exhibit a six-fold symmetry, i.e., the nanowire branches grow along six directions on the hexagonal platelets with an angle of 60° between adjacent branches. With increasing reaction time, the nanowires gradually grew longer, and finer nanowires with an average width and length of approximately 200 nm and 10 μm were obtained (Figs. 2d, g). After the calcination treatment, hierarchical $Co_{3-x}Fe_xO_4$ arrays were obtained. Similarly, hierarchical Co_3O_4 nanosheet@nanorod and hierarchical $Zn_xCo_{3-x}O_4$

nanopillar@nanowire arrays were also fabricated via this one-step self-template growth method by simply adjusting the reaction parameter (Fig. 3) [47].

Although one-step self-template growth approach is facile, the resulted structures of materials greatly depend on the reaction conditions and hard to control. A multi-step-graded growth method involving making secondary structure on a previously obtained primary nanostructure, which can easily combine various methods together to achieve the composite of two or more kinds of compounds, will play well on the issue, because the morphology and structure of final products can be adjusted by the secondary reaction conditions, such as reaction time and temperature, amount of reactants, etc. As far as we know, most of the hierarchical structures were prepared by this approach. For instance, Lee et al. combined chemical vapor with solution-based method for synthesizing MnO_2/SnO_2 hierarchical nanowire [48], and Fan et al. combined hydrothermal synthesis with electrochemical deposition for synthesizing Co_3O_4/NiO core/shell nanowire arrays [52].

We also fabricated several hierarchical arrays by multi-step-graded growth method (Fig. 4). For instance, the synthesis of novel hierarchical Co_3O_4@Ni–Co–O nanosheet@nanorod arrays involved two step hydrothermal reactions and following annealing treatment. (Fig. 4a) [53]. For preparing this hierarchical arrays, Co$(OH)_2$ nanosheet arrays were firstly grown on nickel foam by hydrothermal reactions as previously mentioned. Then, by reacting the obtained Co$(OH)_2$ nanosheet arrays with extra Ni salt and alkali through a secondary hydrothermal process and following annealing treatment, hierarchical Co_3O_4@Ni–Co–O arrays
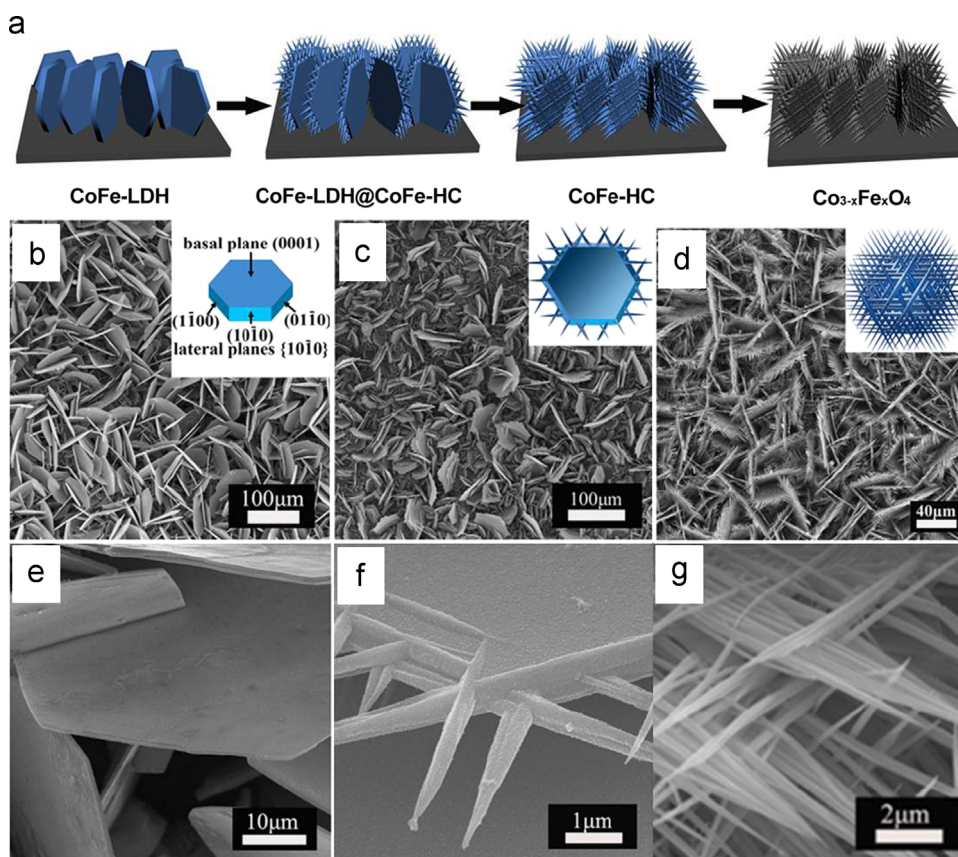
Fig. 2 One-step self-template method for hydrothermal synthesis of hierarchical nanoarrays ($Co_{3-x}Fe_xO_4$ as example). (a) Schematic mechanism of the growth process of hierarchical $Co_{3-x}Fe_xO_4$ arrays on the iron substrate in one pot; SEM images of the products formed at: (b, e) 3 h; (c, f) 4 h; (d, g) 12 h; the insets of b, c and d show schematic illustrations of as-prepared crystallites [19].

involving the growth of densely aligned slim Ni–Co–O nanorods (diameter < 20 nm) on Co_3O_4 nanosheets were fabricated. The thickness of the Ni–Co–O shell on the Co_3O_4 nanosheets could be simply tuned by varying the Ni^{2+} concentration in the second hydrothermal step. Therefore, this method is much flexible to adjust the load mass of activity materials and control the morphology of final products. In addition to this common approach which made secondary structure outside the primary nanostructure, a novel method which made holes inside the primary nanostructure was developed to fabricate mesoporous cobalt carbonate hydroxide (MPCCH) nanosheets with thin structure (Fig. 4b) [54]. The CoAl-LDH nanosheet array was previously synthesized by co-precipitation under hydrothermal conditions on nickel foam. After immersion in 5 M NaOH solution, individual nanosheets became thinner with 3D network maintained. Small holes of several to tens of nanometers in size were clearly observable in the cracked nanosheets, which resulted in mesoporous cobalt carbonate hydroxide (MPCCH) nanosheets.

2.3. Summary

We introduced several strategies for the controlled hydrothermal synthesis of metals oxides and hydroxide nanoarrays. This bottom-up hydrothermal method provides us with many novel synthetic strategies for nanoarrays structures, which has many advantages.

First, since the hydrothermal process occurs irrespective of the kind of materials (Ni, Co, Fe, Zn etc.), this route is very versatile. Second, the process is simple and easily controlled, and we can adjust the morphology, size and structure of nanoarrays by tuning the reaction parameter to satisfy the needs of different applications. More importantly, we can even synthesize multi-metal oxide nanoarrays by reacting two or more kinds of metal salt together in the hydrothermal process. In such a synthetic strategy for nanoarrays, many novel hierarchical arrays were fabricated. Thus, this hydrothermal synthesis method is hence expected to be widely used, and it also offers new opportunities for the design of new types of highly efficient nanoarrays materials.

3. Metal oxide nanoarrays as supercapacitors

Energy storage, an intermediate step to the versatile, clean, and efficient use of energy, has received worldwide concern and increasing research interest [55]. Among the various power source devices, supercapacitors (SCs), also known as electrochemical capacitors, have attracted considerable attention over the past decade due to their high power density, fast charging/discharging rate, and long cycle life comparing to secondary batteries and conventional dielectric capacitors [8,55,56]. In combination with fuel cells or batteries, SCs are anticipated to be useful for powering
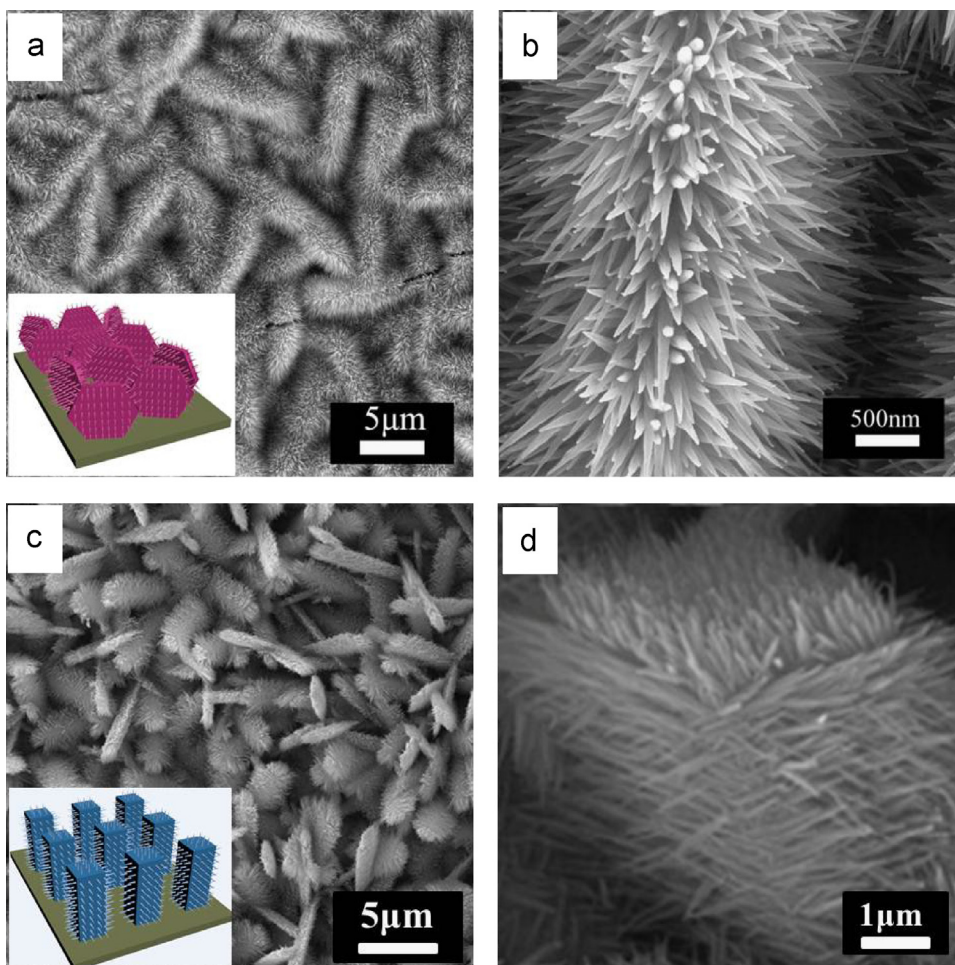
Fig. 3 SEM images of hierarchical Co_3O_4 nanosheet@nanowire (a, b) [47] and $Zn_xCo_{3-x}O_4$ nanopillar@nanowire (c, d) arrays, the insets of a and c are the corresponding schematic illustrations.
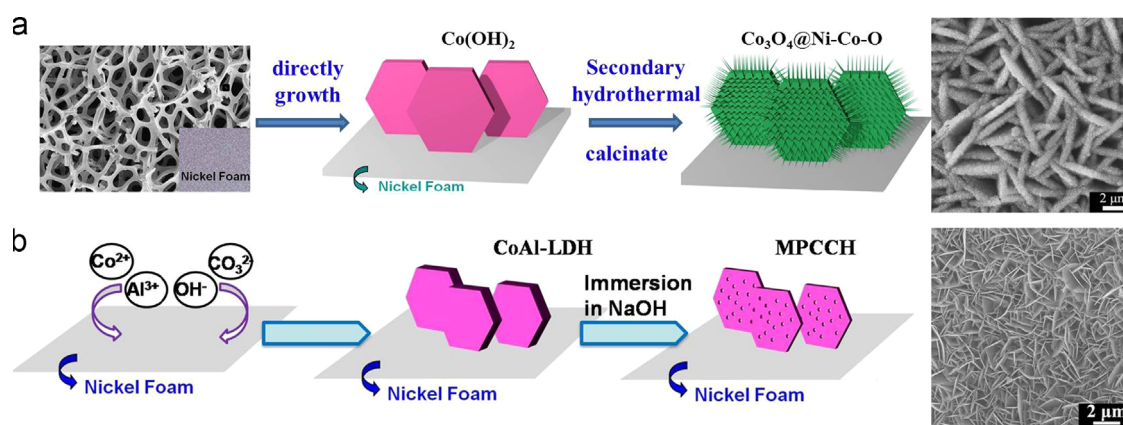
Fig. 4 Schematic diagram of multi-step-graded growth method for hierarchical nanoarrays. (a) Co₃O₄@Ni–Co–O nanosheet@nanorod array; (b) mesoporous cobalt carbonate hydroxide nanosheet array [53,54].

HEVs and EVs, in particular, if the energy density of SCs can be further improved while keeping their high power density unchanged. Generally, SCs can be classified into two types depending on different charge storage mechanisms: traditional electrical double layer capacitors (EDLCs) and pseudo-capacitors. The most commonly used materials for EDLCs are carbonaceous materials including active carbon [57], graphene [58] and carbon nanotubes [59], but the relatively low energy density has limited their applications [8]. In contrast, transition metal oxides or hydroxides with variable valence—such as NiO [60], Co₃O₄ [61–63], MnO₂ [64], Ni(OH)₂ [65], and Co(OH)₂ [66]—can provide higher energy density for supercapacitor. Such materials not only store energy like electrostatic carbon materials but also exhibit electrochemical faradaic reactions between electrode materials and ions within appropriate potential windows [8]. Thus, they often have theoretical specific capacity values larger than 2000 F g^{-1} (e.g. 3560 F g^{-1} for Co₃O₄ [67] and 2573 F g^{-1} for NiO [68]) due to their multiple oxidation states that result in a rich variety of redox reactions for pseudocapacitance generation. However, these materials that previously reported commonly show much lower capacitances, suffer from poor rate capability and/or poor capacitance retention upon cycling.

As well known, the electrochemical activity and kinetic feature of the electrodes play an important role for the performance of SCs. Enhancing the kinetics of ion and electron transportation in electrodes and at the electrode/electrolyte interface can highly improve the power density of SCs. Therefore, constructing electrodes with proper pore structure and good electrical conductivity are highly desirable. On the other hand, by optimizing the structure of electrode materials and designing energy storage devices according to different energy storage mechanisms, the energy density of SCs can be increased. Chen et al. once reviewed the detailed methods to design and synthesize advanced materials for SCs with desirable structures and compositions based on a thorough understanding of the interaction between electrodes and electrolyte ions [55].

Here we introduce several of metal oxides or hydroxides nanoarrays, which meet the general requirements in supercapacitors: (1) the oxide or hydroxides should be electronically conductive; (2) the metal can exist in two or more oxidation states that coexist over a continuous range with no phase changes involving irreversible modifications of a 3-dimensional structure; and (3) the protons can freely intercalate into the oxide/hydroxide lattice on reduction (and out of the lattice on oxidation), allowing facile inter

conversion of $O^{2-} \rightarrow OH^-$. These characteristics are critical for the metal oxides or hydroxide nanoarrays as the promising electrodes for SCs.

3.1. Nanorod array

NiO nanorod array is the first example (Fig. 5) [45]. NiO has received great attention as a supercapacitor material due to its high theoretical specific capacitance (2573 F g^{-1}), well-defined redox behavior, and low cost [60,68,69]. Various NiO nanostructures, including nano-flakes [69], urchin-like structures [70], nanocolumns [60,68], and mesoporous structures [71], have been employed in SCs, but none of them showed stable capacitance larger than 1000 F g^{-1} (after 500 cycles) [51]. Aiming to higher capacitance, we designed a mesoporous ordered architecture by constructing NiO nanorod arrays on Ni foam. Nickel foam was chosen as the substrate due to its high electronic conductivity and a desirable three dimensional (3D) structure. The microholes and zigzag flow channels on the Ni foam substrate provided excellent mass transportation and large surface area per unit area of the electrode [72]. Electrochemical test data demonstrated that a combination of ultrahigh specific capacitance (2018 F g^{-1} at 2.27 A g^{-1}), high power density (1536 F g^{-1} at 22.7 A g^{-1}), and good cycling stability (only 8% of capacitance was lost in the first 100 cycles with no further change in the subsequent 400 cycles) of supercapacitor was achieved. The specific capacitance value exceeds the highest value previously reported for NiO by fully 50%, and is 80% of theoretical value.

It is easy to infer that the high capacitance, high power capacitance and cycling stability could mainly attribute to the well-designed structure of nanoarray: small diameters and the high density of the nanorods, suitable crystallinity, and stable chemical bonding of the NiO nanorods on the Ni substrate. Firstly, the individual NiO nanorod constructing the array has very narrow diameter, smaller than the maximal penetration depth of electrolyte of about 20 nm [73]. This slim rod morphology reduces the diffusion distance through which the electrolyte has to penetrate to less than 10 nm, and thus maximizes the active surface area for insertion and extrusion of OH⁻, as shown schematically in Fig. 5 (e), and consequently maximizes the pseudocapacitance (Fig. 5(e) —Zone 1). At the same time it also maximizes the surface area exposed to the bulk solution, which enlarges the electric double layer capacitance, as shown in the discharge curves

(Fig. 5(e)—Zone 2). Secondly, the 3D porous space between the slim NiO nanorods facilitates the diffusion of electrolytes, and the good crystallinity of the nanorods ensures a good cycling stability and electrical conductivity. In addition, the strong chemical bonding of the rods to the substrate not only ensures good mechanical stability, but also facilitates the transport of electrons from the nanorods to the metallic substrate, the electron collector. Combining all these virtues into one material suggests that this NiO nanorod arrays can be used to fabricate long lifetime, cost-effective and ultrahigh energy/power density SCs.

3.2. Ultrathin nanoarrays

In theory, the mesoporous materials could make full use of both redox reactions at interfaces and the electrical double-layer capacitance from its high surface areas by enlarging the contact area with the electrolyte and enhancing the ion and electron transportation, thus enhance the reversible capacitances, which might be higher than their theoretical pseudocapacitance values. However, this expectation was seldom demonstrated, although there were some reports on the irreversible capacitances higher
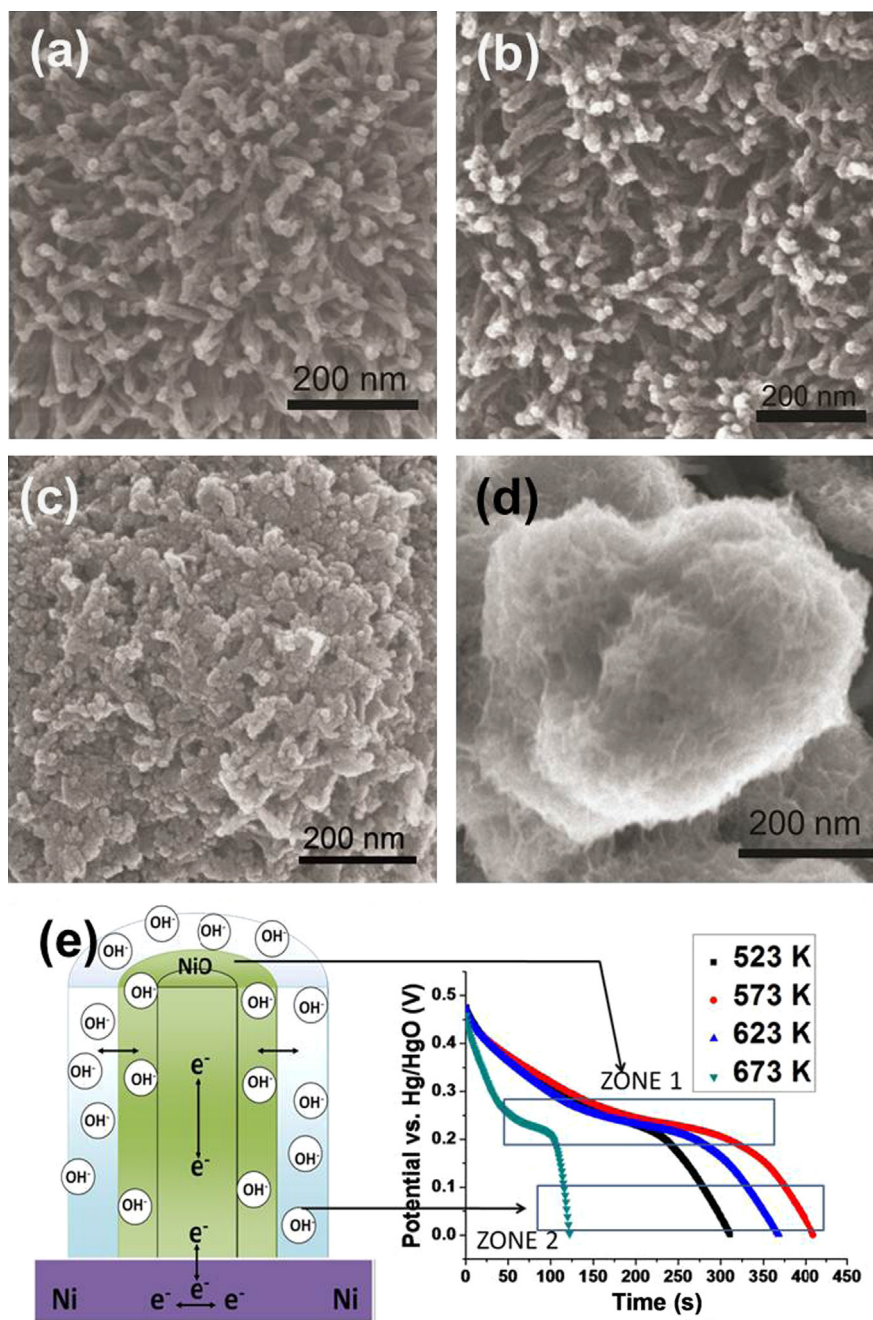
Fig. 5 SEM images of NiO/Ni films after annealing at 523 K (a), 573 K (b), 623 K (c) and 673 K (d); and (e) schematic image shows how the NiO nanorod generates electric double-layer capacitance and pseudocapacitance and the discharge curves with a current density of 5 mA cm^{-2} of the NiO/Ni films calcined at various temperatures [45].

than the theoretical values [46]. Our group recently developed an ultrathin $Ni(OH)_2$ nanowalls film on Ni foam (Figs. 6a–c). This extremely small thickness ($\sim$6 nm) of the nanowalls played an important role in yielding the ultrahigh capacitance by effectively shortening the proton diffusion distance and making the chemically active materials 100% usable for the redox reaction (Fig. 6d). Meanwhile, it also provided additional electrical double layered capacitance at the interfaces. Because of the combination of its Faradic capacitance from full redox reaction at the interfaces and the electrical double-layer capacitance from its high surface area, the $Ni(OH)_2$ nanowalls exhibited an ultrahigh capacitance of 2675 F g^{-1} and 96–98% reversibility depending on the varied current density (5–30 mA cm^{-2}) (Fig.6e). As far as we know, this is the highest capacitance ever reported for a reversible $Ni(OH)_2$ supercapacitor, beyond its theoretical value (2358 F g^{-1} within 0.44 V). Since the EDLC was proportional to the surface area and the voltage decreased as the discharge time extends, while pseudocapacitance involves redox reaction and thus kept a stable voltage (platform), we could distinguish them from the discharge curve. As estimated, the Faradic capacitance section was 2350 F g^{-1}, which was close to theoretical value (2358 F g^{-1}), and the EDLC contribution was 325 F g^{-1}, which meant a specific capacitance per unit surface area (SCs) of 6.08 F m^{-2}, much higher than that of porous carbon (0.1–0.2 F m^{-2}), and near to the usual pseudocapacitances (1–5 F m^{-2}) [55]. The $Ni(OH)_2$ nanowall arrays also showed high cycling stability of capacitance, preserving $>$96% of their original capacitances after 500 cycles and even 102% in the 10 mA cm^{-2} case (Fig. 6f). The ideal combination between ultrahigh specific capacitance and excellent cycling stability made the $Ni(OH)_2$ nanowall film electrode promising for electrochemical energy storage devices. In addition, since the Ni foam was flexible, it could be folded in and out, and thus made into a ring as large as 20 cm^2 to fit a 40 mL

autoclave in lab. Such a feature would be very helpful for a large scale industrial production in future.

Besides that, building mesoporous structure with holes is also an effective method to improve the electrochemical specific surface area of the electrode materials, and thus improves their electrochemical performance (Fig. 7). The mesoporous cobalt carbonate hydroxide (MPCCH) thin nanosheet array from a CoAl-LDH nanosheet following removal of the Al cations by alkali etching were applied in supercapacitor [54]. SEM results indicated that MPCCH preserved its 3D network and porous structure without collapse after alkali etching, but the individual nanosheets became thinner (with thicknesses of ca.10 nm) and showed extensive cracking (e.g. at the edges and the center) (Fig. 7b). This process thinned the sheets, increased the surface area and facilitated the penetration of electrolytes into electrodes. Therefore, the MPCCH was expected to have a much better performance. The maximum specific capacitance of MPCCH could reach 1075 F g^{-1} at 5 mA cm^{-2} (this value is higher than that of previously reported LDH-like pseudocapacitive materials), and 780 F g^{-1} (72%) could be maintained at a much higher current density (50 mA cm^{-2}) (Figs. 7d, f). It is worth noting that the specific capacitance of MPCCH was improved 150% compared with the CoAl-LDH nanosheets, indicating the effective of this method. Additionally, even after 2000 cycles of charge and discharge at 30 mA cm^{-2}, 92% of the initial capacitance could be preserved (Fig. 7e), indicating its high stability.

3.3. Hierarchical nanoarrays

High specific capacitance per area is a critical requirement for a practical supercapacitor electrode, and needs a combination of
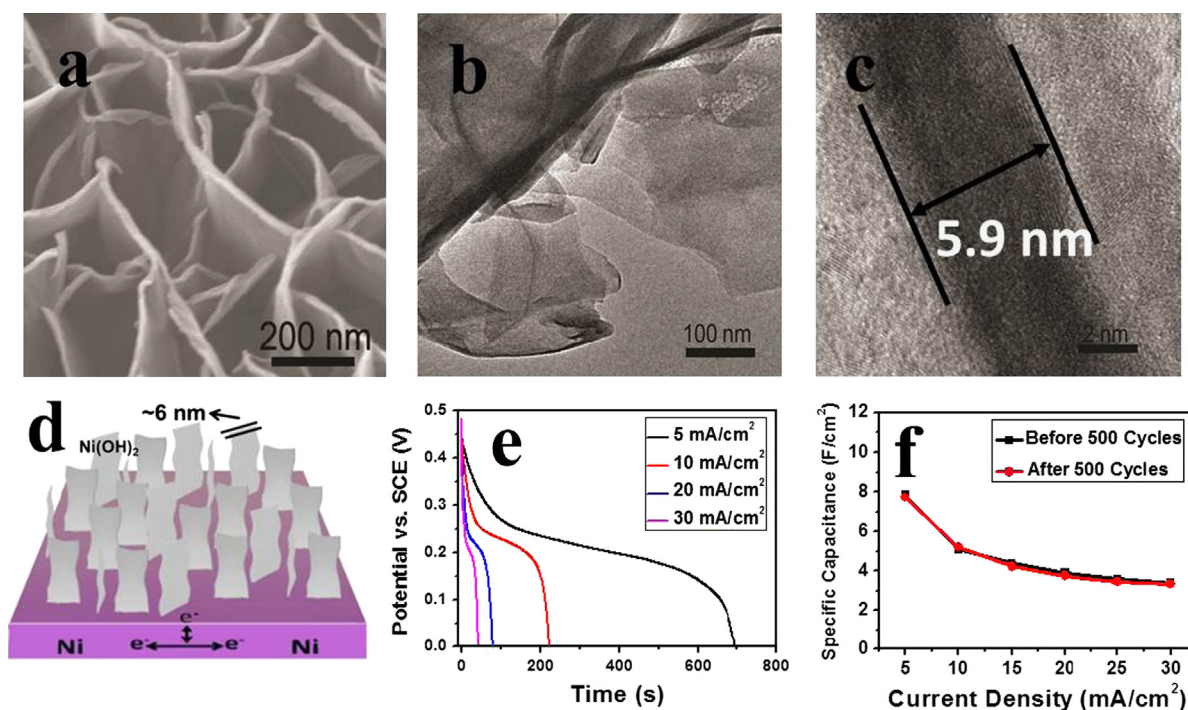

Fig. 6 $Ni(OH)_2$ nanowall films: (a), (b) and (c) are SEM, typical and high-resolution TEM images, respectively; (d) the schematic image; (e) the discharge curves at various current densities; and (f) average specific capacitance versus charge and discharge current density before and after 500 cycles [46].

high mass-loading of the electrochemically active material per area, and high utilization efficiency of this material. However, pursuing high mass-loading on conventional electrodes usually leads to an increase in "dead" material which is not accessible to the electrolyte in the supercapacitor, and thus prevents high utilization efficiencies (as given by the specific capacitance per gram, denoted "SC/g") of the material being realized. It is generally found that the SC/g decreases as the active material per area increases, which results in their specific capacitance per area (SC/A) always being lower than $\sim$15 F cm^{-2} [66,74,75]. These conflicting demands can be understood in terms of the diffusion depth limitation. The diffusion distance of electrolytes into pseudocapacitor electrodes is only $\sim$20 nm in depth [73]. This means that all the material included in such a depth can be considered as "on the surface", and can become involved in the redox reaction, while that underneath is "dead" or "inactive" material as far as electrochemical energy storage is concerned.

Any attempt to increase the mass loading usually results in increasing thickness of material, which consequently leads to more inactive material being buried under the surface, and hence lower overall efficiencies [76].

Recently, this antagonism can be overcome by incorporating the electrochemically active material in a mesoporous hierarchical architecture. It is well accepted that the growth of hierarchical complex nanostructures with multi-dimensions help to avoid many drawbacks in the field of energy storage [7]. The electrochemical performance can be improved by the hierarchical nanostructural design, integrating the high conductivity of the inner core and large surface areas of the outer branches to permit homogeneous interface/chemical distributions at the nanoscale and fast ion and electron transfers. For example, an ultra-high specific capacity (800 F g^{-1}), which is close to its theoretical value was achieved by coating MnO_2 onto SnO_2 nanowires grown on a stainless steel substrate, indicating the high utilization of the materials [64]. In
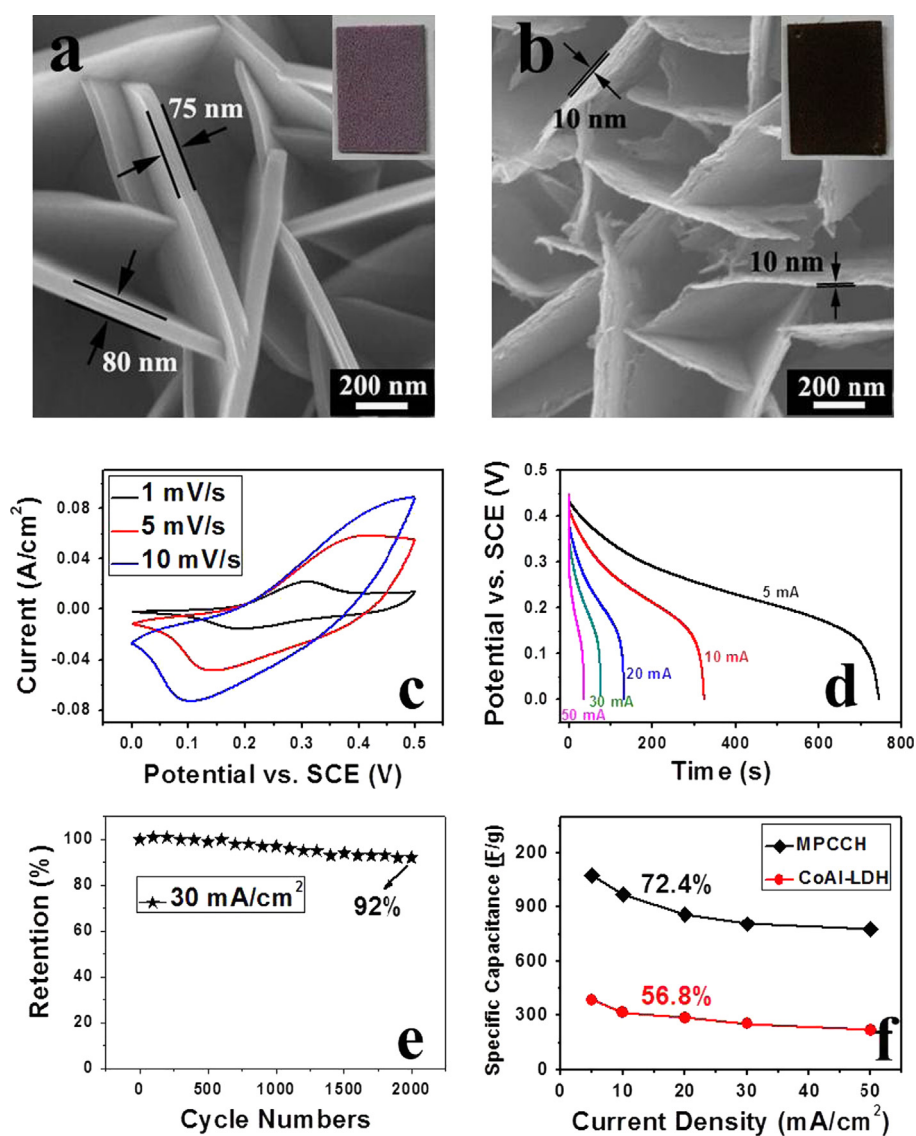

Fig. 7 (a, b) typical SEM images of CoAl-LDH nanosheet array and MPCCH thin nanosheet array after immersing in 5 M NaOH solution overnight (insets are the optical picture). Electrochemical characterization MPCCH thin nanosheet array: (c) CV curves at different scan rates; (d) galvanostatic discharge curves at various discharge current densities; (e) specific capacitance retention versus cycle number at a galvanostatic charge and discharge current density of 30 mA cm^{-2}; and (f) the average specific capacitance versus charge and discharge current density with CoAl-LDH [54].

addition, a hybrid Co_3O_4 core and MnO_2 shell nanowire array exhibited high capacitance with good cycle performance and remarkable rate capability with respect to pure Co_3O_4 arrays as a supercapacitor, especially, the areal capacitance was greatly improved due to the increased load mass of active materials [48]. Very recently, a $Co_3O_4/Co(OH)_2$ core/shell nanowire arrays are evaluated as a supercapacitor cathode material that exhibits high specific capacitances [77].

We also designed several hierarchical nanostructures with controllable dimensions to address this issue. The first example is hierarchical Co_3O_4 nanosheet@nanowire arrays (NSWAs) (as shown in Fig. 8) [47]. By employing this hierarchical design for the electrode, the Co_3O_4 NSWAs with a high load mass (7.6 mg cm^{-2}) provided a high specific capacitance of $715 \, F \, g^{-1}$ (see Fig. 8d), remarkable rate capability (at least 69% can be maintained when the current density increased 6 times), as well as good long-term cycling stability (exactly 100% of its initial specific capacitance after 1000 cycles). Compared with pure Co_3O_4 nanosheet arrays (NSAs) and nanowire arrays (NWAs), hierarchical Co_3O_4 NSWAs showed an improved rate capability over NSAs (58%) and NWAs (42%). It should be noted that although the NWAs exhibited a slightly higher specific capacitance due to the slim morphology, the capacitance decayed very fast with the current density increasing. The high performance of NSWAs including relatively higher capacitance, excellent rate capability and good cycling stability was attributed to the combination of the higher conductivity of the inner nanosheet core and large surface areas of the outer nanowires, which permitted homogeneous interface/chemical distributions at the nanoscale as well as the fast ion and electron transfer (Fig. 8c).

The secondary structure of Co_3O_4 nanosheets is critical in enhancing the specific capacitance. Firstly, the nanosheet provides a 3D scaffold to support the Co_3O_4 nanowires growth, preventing the aggregation during the growth process and electrochemical test. Thus, the nanosheet presents an efficient template for hierarchical hybrid array growth. Secondly, each nanosheet, acting as the base of the hierarchical structure, has its own electric contact with the current collector and thus promotes the conductivity of NSWAs. This ensures that all individuals participate in the electrochemical reaction, which enhances the utilization of the active materials in the electrochemical process, especially in regions far away from the current collector (e.g. tips). Also, the need for binders or conducting additives, which add extra contact resistance or weight, is eliminated. Thirdly, compared with conventional nanowires arrays, open space between neighboring nanowires on the nanosheet is much larger which allows easy diffusion of the electrolyte into the inner region of the electrode, resulting in a high utilization of materials. The larger degree of porosity could enhance the electrolyte/Co_3O_4 contact area and the open space between neighboring nanowires allow easy diffusion of the electrolyte, which may lead to high power applications when the sample is charged or discharged at high current. In other words, better rate capability can be achieved. Fourthly, the synergistic effect of nanosheet and nanowire is critical to high capacitive performance as mentioned above. Additionally, the hierarchical array possesses a
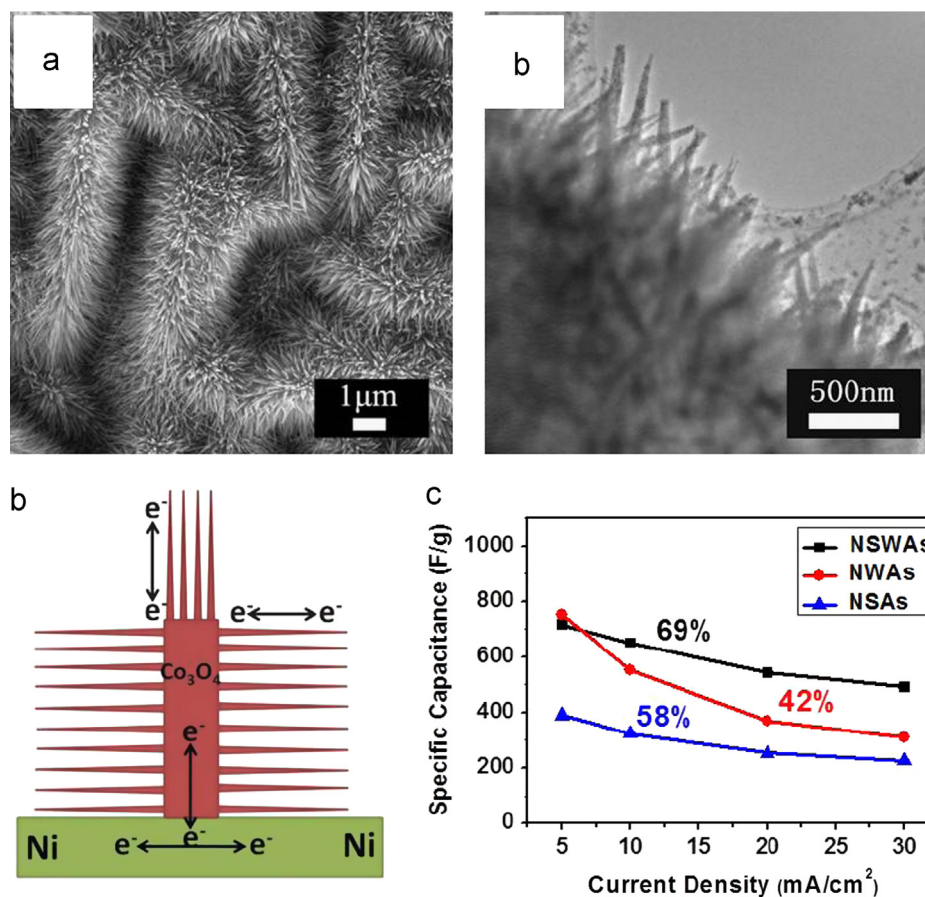
Fig. 8 (a, b) Typical SEM and TEM images of Co_3O_4 NSWAs; (c) schematic image of the electron transmission in hierarchical structure; and (d) specific capacitance versus current densities of NSWAs, NSAs and NWAs [47].

favorable morphological and phase stability, which helps to alleviate the structure or phase damage caused by volume expansion and redox reaction during the cycling process. This unique structure lead to enhanced capacitance and rate capability of the Co_3O_4 NSWAs compared with the bare Co_3O_4 nanosheet arrays.

However, the performance of Co_3O_4 NSWAs was restricted by the relatively large size of the secondary structure (the nanowires, $\sim$80 nm in diameter), which does not fit to the threshold diffusion depth ($\sim$20 nm). Hence, we fabricated hierarchical Co_3O_4 nanosheet@Ni–Co–O nanorod arrays as a supercapacitor electrode (Fig. 9) [53]. The uniform and slim tertiary Ni–Co–O nanorods were only $\sim$10 nm in diameter, which exposed all of the material to the electrochemically active surface layer and ensured high utilization efficiency (Fig. 9b). At a current density of 5 mA cm^{-2}, the unique hierarchical structure of NSRAs allowed the supercapacitor electrode to have an extremely high mass loading per area (12 mg cm^{-2}) and high efficiency of 2098 F g^{-1}, giving specific capacitances per area as high as $\sim$25 F cm^{-2} (Figs. 9d, e). For the similar structure Co_3O_4/NiO core/shell, their capacitance can only reach to 853 F g^{-1} at 2 A g^{-1} [52]. When the current density was increased from 5 mA cm^{-2} to 30 mA cm^{-2}, 72% of the specific capacitance was retained and, furthermore, no significant decrease in capacitance was observed over 1000 charge/discharge cycles (Figs. 9f, g). The combination of these merits made the composite material an excellent candidate for practical application as a supercapacitor electrode and, more generally, highlights the increased efficacies of materials that could be obtained from fabricating mesoporous hierarchical structures at the nanoscale.

Recently, this design concept is extended to the research field of LDH nanomaterials. Wei et.al reported CoAl-layered double hydroxide (LDH)@poly (3, 4-ethylenedioxythiophene) (PEDOT) nanoplatelets with core/shell structure on a flexible Ni foil substrate as a high-performance pseudocapacitor. The synergistic effect of individual components played a key role in determining the high-performance of the LDH@PEDOT NPA electrode. The LDH nanoplatelet core provided abundant energy-storage capacity, while the highly conductive PEDOT shell and porous architecture facilitated the electron/mass transport in the redox reaction [50]. They also prepared hollow NiAl-LDH microspheres with tunable interior architecture, which exhibited excellent pseudocapacitance performance, owing to the greatly improved faradaic redox reaction and mass transfer. Therefore, these works provide a promising approach for the design and synthesis of hierarchical structure materials with largely enhanced supercapacitor behavior, which can be potentially applied in energy storage/conversion devices [49].

3.4. Summary

We summarize and compare the performance of metal oxide or hydroxide nanoarrays pseudo-capacitors prepared in our group with the ones reported in the literature in Table 1. All our samples show excellent electrochemical performance, including high capacitance, remarkable rate capability and excellent cycling performance, which make them promising candidates for practical application as supercapacitor electrodes.

There are several factors that affect the pseudocapacitance of electrodes. First, the morphology plays a determinant role in electrochemical performance. The morphology of electrodes closely relates to the specific surface area and pore structure. Generally, the specific capacitance of a material will increase significantly as its surface area increases. Larger surface area means more faradaic active sites and thereby higher pseudocapacitance. Furthermore, high porosity can easily relieve the internal stress created during the charging and discharging processes, thus protects the electrode from physical damage. The second one is crystallinity. If the crystallinity is too high, the protonation (or deprotonation) reaction will be limited. Although high crystallinity helps increase of higher conductivity, loss of surface area occurs simultaneously. However, lower crystallinity could lead to a low electrical conductivity of the electrodes, due to its tendency of forming highly porous microstructure. Therefore, there should be a trade-off between electrical conductivity in the solid phase and ionic transport in the pore.

Our recent progress suggests that the hierarchical design of the nanoarrays takes advantages of the synergistic effect of the nanocomponents at different scales, in which the minimum level structures provide a highly porous and large surface area and the first and second level structures with high crystallinity in micron scale ensure the high conductivity in the electrodes. With above design, a high specific capacitance, good rate characteristic and long-term life for supercapacitor can be achieved. These studies are of great importance in the development of a practical supercapacitor electrode because it offers a material with a combination of ultra-high specific capacitance, high power capacitance, and high stability, together with low cost, simple procedures, and high reproducibility.

4. Catalytic applications of mixed metal oxide nanoarrays

As we know, catalysts, especially when they are applied in a structured way, play important roles in the so-called integrated approach to industrial catalysis and environmental protection. Their advantages such as small pressure drop, good mechanical stability and easy catalyst separation make them superior to conventional powder catalysts [78,79]. However, there are still some disadvantages limiting their practical applications. One is that the active components often distribute irregularly and is easy to lose during catalytic reactions. Generally, a structured catalyst is made by applying a layer of a catalytically active component to the walls (or inside the walls) of an inert monolith structure. A homogeneous distribution of the active component on the monolith is often difficult to achieve [80]. Also, good adhesion of the active material to the substrate could be a problem so that leaching occurs during catalytic reactions in solvents.

The developments of nanoarrays in electronic/electrochemical electrodes in recent decades triggered our thoughts to use hierarchical nanoarrays as candidates for new-style structured catalysts because they can offer structured advantages in multiple scales. In macroscale, with the catalytically active component directly grown on a substrate, we can realize the catalyst immobilization and also get a homogeneous distribution of the active material, ideally allowing its catalytic properties to be maintained even under harsh reaction conditions. In mesoscopic scale, the specific surface area of the catalysts can be increased by the design of a hierarchical structure, thus enhancing the accessibility of the reactant to the catalytic site and favouring molecular diffusion and material transfer. As we know, the heterogeneous catalysis is a typical surface process and the surface atoms of catalysts mainly determine the kinetics of the reactions. Therefore, nanostructure catalysts are more powerful in tuning the surface structure and atomic arrangement of catalyst, and are expected to exhibit better catalytic performance [81]. Furthermore, in
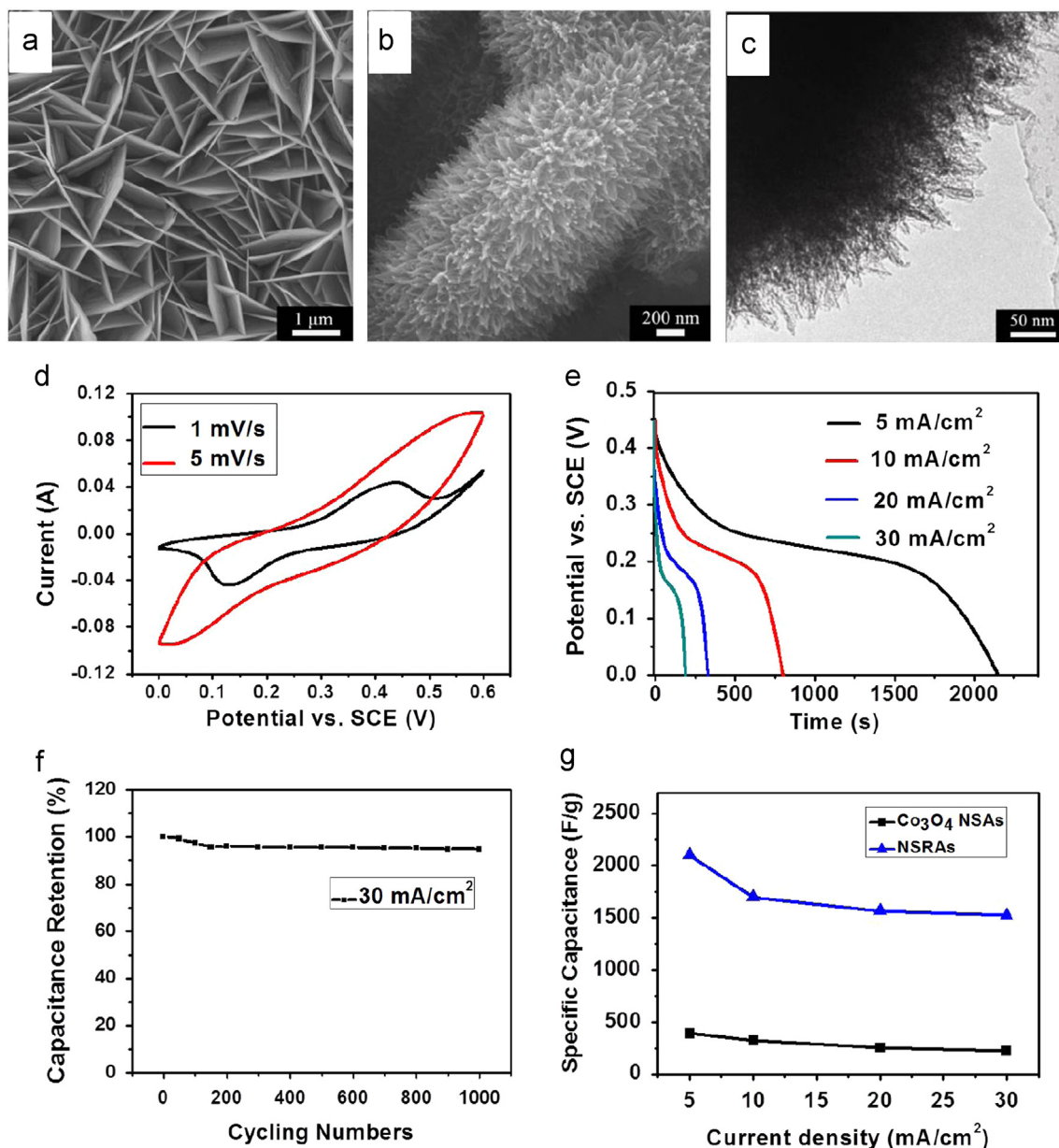
Fig. 9 (a) Typical SEM image of Co_3O_4 nanosheet array; (b) and (c) Typical SEM and TEM images of NSRAs. Electrochemical characterization of NSRAs: (d) CV curves at different scan rates; (e) galvanostatic discharge curves at various discharge current densities; (f) average specific capacitance versus cycle number at a galvanostatic charge and discharge current density of 30 mA cm^{-2}; and (g) plots of specific capacitance per gram versus current density with Co_3O_4 NSAs [53].

microscopic scale, the exposed crystal planes of nanocatalysts determine, to a great extent, their catalytic properties including activity and selectivity. For instance, Co_3O_4 nanostructures with different dominant exposed planes show different catalytic activities for the combustion of methane and CO oxidation [82]. Hence, it is very desirable to synthesize nanocatalysts with high ratios of more reactive crystal planes (we called the total surface area of reactive crystal planes as "effective surface area"). By making uniform nanoarray with more reactive crystal planes exposed, we could improve the "effective surface area", and finally enhance the catalytic activity of the catalyst. With these ideas, a uniform hierarchical nanoarray with more reactive crystal planes exposed, directly grown on a metal substrate, should be an effective architecture for a structured catalyst. On the other hand, mixed metal oxides, due to the effect of doping metal, can improve the properties of materials, when compared with single-metal oxides. For example, Ni doped cobalt-based oxide ($Ni_xCo_{3-x}O_4$) has better catalytic performance for oxygen evolution on reaction than the pure Co_3O_4 electrodes, because the doping amount of Ni element have a great effect on the morphology and structure of the electrodes materials, thus, influences the surface roughness, resulting in the different catalyst performance [72].

4.1. Hierarchical $Co_{3-x}Fe_xO_4$ arrays

Our first example is hierarchical cobalt iron oxide nanoarrays and their catalytic activity in the oxidation of alkenes by organic

Table 1 Comparison of the capacity (at low and high current densities) and capacity retention of the materials in our group (marked "*") with the ones reported in the literature.

| Material	Capacity (F g^{-1}) (low current densities)	Capacity (F g^{-1}) (high current densities)	Capacity retention
*NiO nanorod [45]	2018 (5 mA cm^{-2})	1536 (30 mA cm^{-2})	92% (500 cycles)
*Ni(OH)$_2$ nanowall [46]	2675 (5 mA cm^{-2})	1150 (30 mA cm^{-2})	96% (500 cycles)
*MPCCH [54]	1075 (5 mA cm^{-2})	805 (30 mA cm^{-2})	92% (2000 cycles)
*Hierarchical Co$_3$O$_4$ [47]	715 (5 mA cm^{-2})	491 (30 mA cm^{-2})	100% (1000 cycles)
*Co$_3$O$_4$@Ni$_3$-Co-O [53]	2098 (5 mA cm^{-2})	1525 (30 mA cm^{-2})	96% (1000 cycles)
NiO flake [69]	942 (5 mA cm^{-2})	613 (39 mA)	98% (500 cycles)
Ni(OH)$_2$/GS [65]	1335 (2.8 A g^{-1})	953 (45.7 A g^{-1})	100% (2000 cycles)
Co$_3$O$_4$ nanoflowers [62]	1309 (3 A g^{-1})	900 (10 A g^{-1})	98% (500 cycles)
Co$_3$O$_4$ nanosheet [63]	2735 (2 A g^{-1})	1471 (10 A g^{-1})	99% (3000 cycles)
LDH@PEDOT [50]	672 (1 A g^{-1})	424 (40 A g^{-1})	92% (5000 cycles)
NiCo$_2$O$_4$ nanoneedle [17]	1118 (5 mA cm^{-2})	656 (11 mA cm^{-2})	90% (2000 cycles)
Co$_3$O$_4$/NiO core/shell [52]	452 (2 A g^{-1})	384 (40 A g^{-1})	95% (6000 cycles)

peroxides [19]. This hierarchical Co$_{3-x}$Fe$_x$O$_4$ nanoarray was prepared as we mentioned in Section 2, which showed high catalytic activity (92.2% conversion) and selectivity (64.6% for benzaldehyde) for styrene oxidation by tert-butyl hydroperoxide (TBHP). This value was higher than the one of Co$_3$O$_4$ nanorod arrays (about 30% styrene conversion after 3 h, and 75% conversion after 12 h) and catalysts reported in the literature [83–85] (Fig. 10a). Furthermore, the hierarchical cobalt iron oxide nanoarrays showed excellent cycling stability for styrene oxidation (Fig. 10b). The activity and the selectivity of recycled catalyst were almost equal to the fresh catalyst and there are no any significant morphology and structural changes in the catalyst after the catalyst being used for nine times (Figs. 10c, d).

Their excellent catalytic activity and stability for styrene oxidation can be related to the preferential exposure of crystal planes with a relatively high density of active species (i.e. $\{1\bar{1}2\}$), the doping of Fe in situ, and the hierarchical design of the nanoarray. First, the direct growth of hierarchical nanostructure on substrate avoids the irregular distribution of the active component that tends to occur in traditional coating process and ensures the strong anchor of the catalyst thus mitigating leaching during the catalytic reactions. Second, hierarchical structure provides large surface area which resulted in a high utilization of materials, and the open spaces between individual nanocrystals can also facilitate the diffusion of gas and mass transport. The precursor LDH nanosheets play a critical role. They first provide a 3D scaffold to support the growing nanowires. So that can give a rough surface to grow second nanostructures with a large surface area and prevent aggregation during the process. The enhancement of the surface area was confirmed by the measurement of electrochemical surface areas. The roughness factors of the materials increased from 3 to around 2538. The results indicate considerable increase occurs on their surface area in the stepwise growth process. Also, LDH platelets were used as a template for the growing of the secondary nanowires. This makes the resulted cobalt iron oxide nanowires mainly exposes the $\{1\bar{1}2\}$ planes. These planes happen to be the high active one of Co$_3$O$_4$ due to the exposure of more active trivalent cobalt ion sites. Theoretical calculations using the density functional theory (DFT) method for different surfaces confirm that styrene and TBHP molecules interact preferably with the $\{1\bar{1}2\}$ planes, since their adsorption energies are more favorable than on other crystal planes (see Figs. 10e–i). The surface area of $\{1\bar{1}2\}$ planes is estimated to contribute 71% of the total surface area,

which means we have created more "effective surface area" in the catalyst. Moreover, the nanosheets also act as a connecting buffer between the macroscale substrate and the nanoscale nanowires, and thus can ensure efficient anchoring of the nanowires. Finally, it should be noted that Fe doping enhances the catalytic efficiency of Co$_3$O$_4$. The structure of Co$_{3-x}$Fe$_x$O$_4$ transforms from normal spinel into inverse spinel as x increases, which leads to the appearance of new active sites in the samples—Fe^{3+} ions in octahedral coordination increase the mobility of the reactive oxygen. Another advantage of nanoarray is the flexibility of its shape. It can be molded into the desired shape for a particular catalytic reactor, such as rolling into a cylindrical form. So it could be directly used in the catalytic reaction in the form of structured catalyst.

4.2. Hierarchical Zn$_x$Co$_{3-x}$O$_4$ arrays

After the work on cobalt iron oxide nanoarrays for selective oxidation of alkene, we extended the study to the oxygen evolution reaction (OER). OER is involved in many electrochemical processes, such as water splitting for hydrogen production and reducing CO$_2$ to fuels. An effective electrocatalyst can reduce the overpotential and thus enhance the energy efficiency. Up to date, the most extensively studied catalysts for this reaction are nanostructured IrO$_2$ and RuO$_2$ [86–88], but they are expensive and very rare. Well-aligned nanoarrays with the catalytically active component directly grown on a conductive substrate generally exhibit many advantages such as good electrical conductivity, low diffusion resistance to ionic species, and easy electrolyte penetration, thus offered the possibility to fabricate novel OER catalysts with high reactivity and stability.[33,72] This triggered our thoughts of developing kind of non-noble metal catalyst using hierarchical nanoarrays. We prepared hierarchical Zn$_x$Co$_{3-x}$O$_4$ nanopillar@nanowire arrays, which were assembled with nanowires on Ti substrates and studied their electrocatalytic performance for OER. This hierarchical structure provided good electron transportation capability, efficient mass transfer, and large surface area. Therefore, the resulting Zn$_x$Co$_{3-x}$O$_4$ arrays exhibited excellent OER electrocatalytic activity in basic media, and afforded a current density of 10 mA cm^{-2} at a small overpotential of ~0.32 V and a small Tafel slope of 52 mV/decade (Fig. 11), comparable to the performance of the best reported Co-based oxides OER
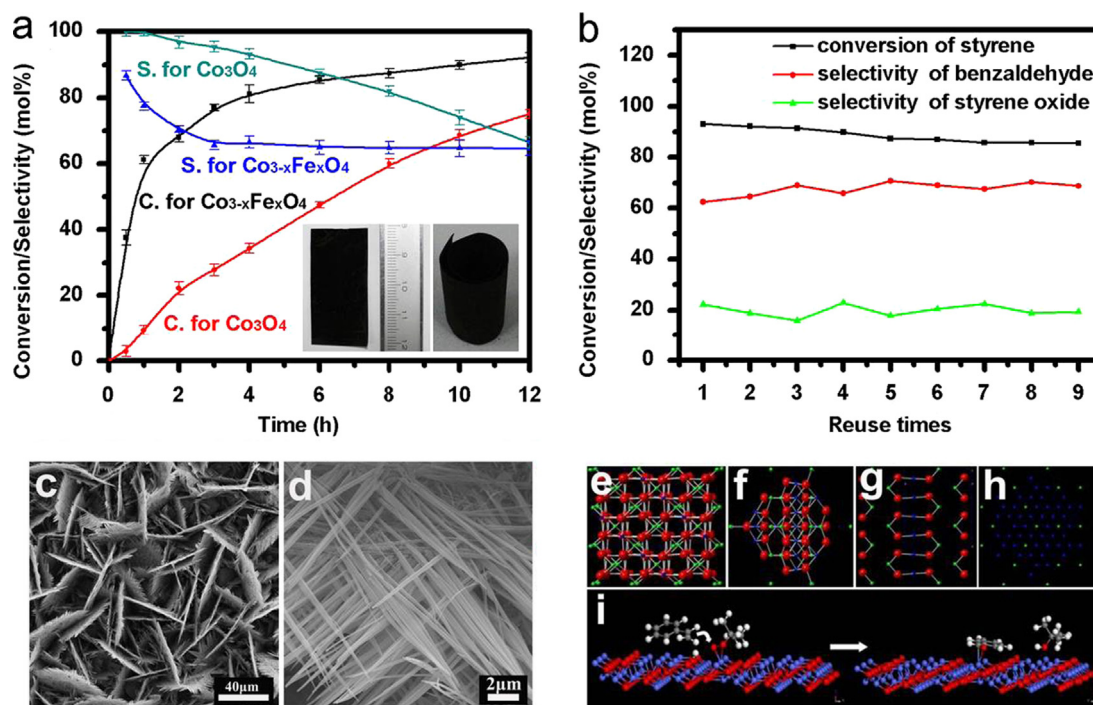
Fig. 10 (a) Effect of varying the reaction time on styrene conversion and benzaldehyde selectivity for $Co_{3-x}Fe_xO_4$ and Co_3O_4 catalysts, inset: optical images of film of $Co_{3-x}Fe_xO_4$ nanoarrays (left) and in the form of structured catalyst (right); (b) the recyclability of the $Co_{3-x}Fe_xO_4$ nanoarray structured catalyst; (c), (d) SEM images of $Co_{3-x}Fe_xO_4$ nanoarrays at different magnifications after being used nine times; (e) spinel structure of Co_3O_4; (f–h) the surface atomic configurations in the $\{1\overline{1}2\}$, $\{110\}$, and $\{1\overline{1}1\}$ planes; and (i) a schematic diagram for TBHP adsorption and styrene oxidation on the active Co^{3+} sites. The red, gray, white and blue spheres are oxygen atoms, carbon atoms, hydrogen atoms and cobalt atoms, respectively [19].

catalyst and commercial Pt/C (20% Pt on Vulcan XC-72) catalyst. Their high performances should attribute to the high porosity and through-pore structure, which is favorable for electrolyte penetration and fast ion/electron transfer and may lead to enhanced electrochemical reactivity.

4.3. Summary

The strategy of constructing structured catalysts with hierarchical nanoarrays offers new opportunities for developing new types of highly efficient catalysts, which show many advantages. First, the uniform nanoarray directly grown on a metal substrate achieve the homogeneous distribution of active material, and avoid leaching occurs during catalytic reactions in solvents. Second, the hierarchical porous architecture of the materials enhances the accessibility of the reactant to the catalytic site and favouring molecular diffusion, and provides the catalyst with high activity and especially the good cycling stability. Finally, nanoarrays with more reactive crystal planes exposed exhibit high selective, which also open up new opportunities for molecular-level studies in heterogeneous catalysis. In all, nanoarray structured materials, due to the large active surface area, high utilization efficiency of active materials, and superior mass transport property, is particularly beneficial for the catalysis. This concept is helpful to explore the development of new high performance structured catalyst, and have a great significance in developing the green chemical process.

5. Conclusions and perspectives

This article provides an overview of some recent developments in our group related to hydrothermal synthesis of metal oxide and hydroxide nanoarrays directly on metal substrates, aiming to the application on SCs and catalysts. Compared with physical methods and gas-phase strategies, the hydrothermal routes are much more easily controlled and can produce nanoarrays in a designed structure and morphology. Several general strategies for making advanced materials for SCs and catalysis have been developed, such as nanostructuring, nano-/microcombination, pore structure control, hierarchical design, and novel device design. We foresee that the approaches described here will be extended to more oxide systems. Looking ahead, hierarchical nanoarrays with high capacity/activity, long cycling life, good safety, and good reliability will undoubtedly boost the performance of energy storage devices and catalyst constructed on them and certainly gives a great impetus to their wide applications. This design concept can also direct the fabrication of multifunctional hybrid nano- and microstructures, which will be promising for a large spectrum of device applications.
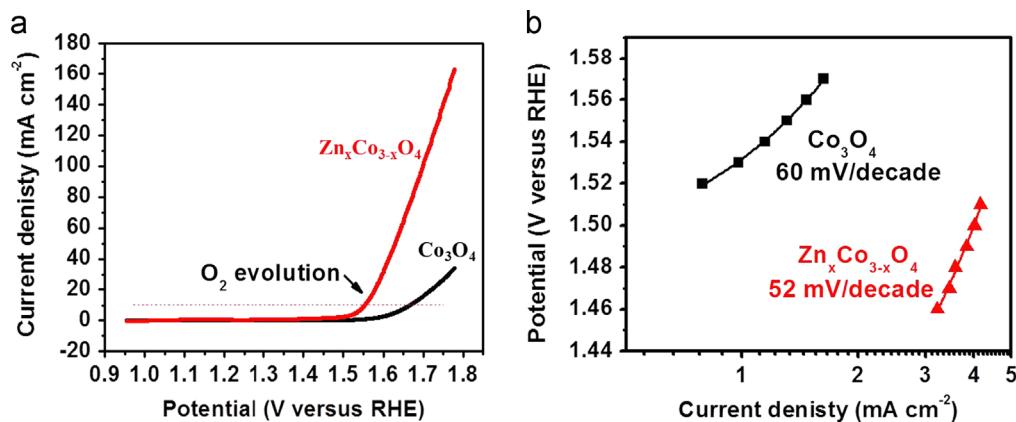
Fig. 11 (a) Steady state polarization curves of Co_3O_4 and $Zn_xCo_{3-x}O_4$ electrodes recorded at the scan rate of 0.5 mV s^{-1} and (b) represents the corresponding Tafel plots.

References

[1] F. Gu, L. Zhang, X. Yin, L. Tong, Nano Letters 8 (2008) 2757–2761.

[2] S. Li, Z. Yu, S.F. Yen, W. Tang, P.J. Burke, Nano Letters 4 (2004) 753–756.

[3] S. Kar, B. Satpati, P. Satyam, S. Chaudhuri, Journal of Physical Chemistry B 109 (2005) 19134–19138.

[4] M. Ohwada, K. Kimoto, K. Suenaga, Y. Sato, Y. Ebina, T. Sasaki, Journal of Physical Chemistry Letters 2 (2011) 1820–1823.

[5] G. Zhu, Z. Xu, Journal of the American Chemical Society 133 (2011) 148–157.

[6] R.K. Joshi, J.J. Schneider, Chemical Society Reviews 41 (2012) 5285–5312.

[7] J. Jiang, Y. Li, J. Liu, X. Huang, C. Yuan, X.W.D. Lou, Advanced Materials 24 (2012) 5166–5180.

[8] G. Wang, L. Zhang, J. Zhang, Chemical Society Reviews 41 (2012) 797–828.

[9] D. Wang, T. Xie, Y. Li, Nano Research 2 (2009) 30–46.

[10] Y. Kang, X. Ye, J. Chen, Y. Cai, R.E. Diaz, R.R. Adzic, E.A. Stach, C.B. Murray, Journal of the American Chemical Society 135 (2013) 42–45.

[11] W. Wu, S. Zhang, F. Ren, X. Xiao, J. Zhou, C. Jiang, Nanoscale 3 (2011) 4676–4684.

[12] W.N. Wang, W.J. An, B. Ramalingam, S. Mukherjee, D.M. Niedz-wiedzki, S. Gangopadhyay, P. Biswas, Journal of the American Chemical Society 134 (2012) 11276–11281.

[13] J.H. Shim, Y. Lee, M. Kang, J. Lee, J.M. Baik, C. Lee, M.H. Kim, Analytical Chemistry 84 (2012) 3827–3832.

[14] Y. Liu, Z. Kang, Z. Chen, I. Shafiq, J. Zapien, I. Bello, W. Zhang, S. Lee, Crystal Growth and Design 9 (2009) 3222–3227.

[15] C. Li, G. Hong, P. Wang, D. Yu, L. Qi, Chemistry of Materials 21 (2009) 891–897.

[16] M.L. Zhang, X. Fan, H.W. Zhou, M.W. Shao, J.A. Zapien, N.B. Wong, S.T. Lee, Journal of Physical Chemistry C 114 (2010) 1969–1975.

[17] G.Q. Zhang, H.B. Wu, H.E. Hoster, M.B. Chan-Park, X.W. Lou, Energy and Environmental Science 5 (2012) 9453–9456.

[18] J.N. Tiwari, R.N. Tiwari, K.S. Kim, Progress in Materials Science 57 (2012) 724–803.

[19] J. Sun, Y. Li, X. Liu, Q. Yang, J. Liu, X. Sun, D.G. Evans, X. Duan, Chemical Communications 48 (2012) 3379–3381.

[20] W. Xiao, D. Wang, X.W. Lou, Journal of Physical Chemistry C 114 (2009) 1694–1700.

[21] V. Bajpai, L. Dai, T. Ohashi, Journal of the American Chemical Society 126 (2004) 5070–5071.

[22] H. Ogihara, M. Sadakane, Y. Nodasaka, W. Ueda, Chemistry of Materials 18 (2006) 4981–4983.

[23] M. McCune, W. Zhang, Y. Deng, Nano Letters 12 (2012) 3656–3662.

[24] X. Feng, K. Shankar, O.K. Varghese, M. Paulose, T.J. Latempa, C.A. Grimes, Nano Letters 8 (2008) 3781–3786.

[25] G. Zhu, Z. Qu, G. Zhuang, Q. Xie, Q. Meng, J. Wang, Journal of Physical Chemistry 115 (2011) 14806–14811.

[26] J.H. Zhong, G.R. Li, Z.L. Wang, Y.N. Ou, Y.X. Tong, Inorganic Chemistry 50 (2011) 757–763.

[27] X. Wang, X. Li, X. Sun, F. Li, Q. Liu, Q. Wang, D. He, Journal of Materials Chemistry 21 (2011) 3571–3573.

[28] Y. Shi, H.Y. Li, L. Wang, W. Shen, H.Z. Chen, ACS Applied Materials and Interfaces 4 (2012) 4800–4806.

[29] Y. Qu, L. Liao, Y. Li, H. Zhang, Y. Huang, X. Duan, Nano Letters 9 (2009) 4539–4543.

[30] Z. Zhang, S. Dai, D.A. Blom, J. Shen, Chemistry of Materials 14 (2002) 965–968.

[31] C. Yan, X. Li, K. Zhou, A. Pan, P. Werner, S.L. Mensah, A.T. Vogel, V. Schmidt, Nano Letters 12 (2012) 1799–1805.

[32] C.K. Chan, H. Peng, G. Liu, K. McIlwrath, X.F. Zhang, R.A. Huggins, Y. Cui, Nature Nanotechnology 3 (2007) 31–35.

[33] Y. Li, P. Hasin, Y. Wu, Advanced Materials 22 (2010) 1926–1929.

[34] T. Bhuvana, G. Kulkarni, ACS Nano 2 (2008) 457–462.

[35] J.P. Ge, J. Wang, H.X. Zhang, Y.D. Li, Chemistry—A European Journal 10 (2004) 3525–3530.

[36] Y. Yin, A.P. Alivisatos, Nature 437 (2004) 664–670.

[37] R. Jin, Y.W. Cao, C.A. Mirkin, K. Kelly, G.C. Schatz, J. Zheng, Science 294 (2001) 1901–1903.

[38] K. Saron, M. Hashim, Superlattices and Microstructures 56 (2013) 55–63.

[39] J. Yun, T.S. Bae, J.D. Kwon, S. Lee, G.H. Lee, Nanoscale 4 (2012) 7221–7230.

[40] S. Zhou, L. Liu, S. Lou, Y. Wang, X. Chen, H. Yuan, Y. Hao, R. Yuan, N. Li, Applied Physics A 102 (2011) 367–371.

[41] R.E. Sabzi, K. Kant, D. Losic, Electrochimica Acta 55 (2010) 1829–1835.

[42] A. Wei, X.W. Sun, J. Wang, Y. Lei, X. Cai, C.M. Li, Z. Dong, W. Huang, Applied Physics Letters 89 (2006) 123902–123902-3.

[43] Y. Zhou, H. Li, Journal of Materials Chemistry 12 (2002) 681–686.

[44] W. Shi, S. Song, H. Zhang, Chemical Society Reviews 42 (2013) 5714–5743, http://dx.doi.org/10.1039/c3cs60012b.

[45] Z. Lu, Z. Chang, J. Liu, X. Sun, Nano Research 4 (2011) 658–665.

[46] Z. Lu, Z. Chang, W. Zhu, X. Sun, Chemical Communications 47 (2011) 9651–9653.

[47] Q. Yang, Z. Lu, Z. Chang, W. Zhu, J. Sun, J. Liu, X. Sun, X. Duan, RSC Advances 2 (2012) 1663–1668.

[48] J. Liu, J. Jiang, C. Cheng, H. Li, J. Zhang, H. Gong, H.J. Fan, Advanced Materials 23 (2011) 2076–2081.

[49] M. Shao, F. Ning, Y. Zhao, J. Zhao, M. Wei, D.G. Evans, X. Duan, Chemistry of Materials 24 (2012) 1192–1197.

[50] J. Han, Y. Dou, J. Zhao, M. Wei, D.G. Evans, X. Duan, Small 9 (2013) 98–106.

[51] J.H. Kim, K. Zhu, Y. Yan, C.L. Perkins, A.J. Frank, Nano Letters 10 (2010) 4099–4104.

[52] X. Xia, J. Tu, Y. Zhang, X. Wang, C. Gu, X.-B. Zhao, H.J. Fan, ACS Nano 6 (2012) 5531–5538.

[53] Z. Lu, Q. Yang, W. Zhu, Z. Chang, J. Liu, X. Sun, D.G. Evans, X. Duan, Nano Research 5 (2012) 369–378.

[54] Z. Lu, W. Zhu, X. Lei, G.R. Williams, D. OHare, Z. Chang, X. Sun, X. Duan, Nanoscale 4 (2012) 3640–3643.

[55] C. Liu, F. Li, L.P. Ma, H.M. Cheng, Advanced Materials 22 (2010) E28–E62.

[56] P. Simon, Y. Gogotsi, Nature Materials 7 (2008) 845–854.

[57] K. Jurewicz, K. Babel, Energy and Fuels 24 (2010) 3429–3435.

[58] C. Liu, Z. Yu, D. Neff, A. Zhamu, B.Z. Jang, Nano Letters 10 (2010) 4863–4868.

[59] K.H. An, W.S. Kim, Y.S. Park, J.M. Moon, D.J. Bae, S.C. Lim, Y.S. Lee, Y.H. Lee, Advanced Functional Materials 11 (2001) 387–392.

[60] C. Yuan, X. Zhang, L. Su, B. Gao, L. Shen, Journal of Materials Chemistry 19 (2009) 5772–5777.

[61] Y. Gao, S. Chen, D. Cao, G. Wang, J. Yin, Journal of Power Sources 195 (2010) 1757–1760.

[62] X. Qing, S. Liu, K. Huang, K. Lv, Y. Yang, Z. Lu, D. Fang, X. Liang, Electrochimica Acta 56 (2011) 4985–4991.

[63] C. Yuan, L. Yang, L. Hou, L. Shen, X. Zhang, X.W.D. Lou, Energyand Environmental Science 5 (2012) 7883–7887.

[64] J. Yan, E. Khoo, A. Sumboja, P.S. Lee, ACS Nano 4 (2010) 4247–4255.

[65] H. Wang, H.S. Casalongue, Y. Liang, H. Dai, Journal of the American Chemical Society 132 (2010) 7472–7477.

[66] J.K. Chang, C.M. Wu, I.W. Sun, Journal of Materials Chemistry 20 (2010) 3729–3735.

[67] Y. Wang, Z. Zhong, Y. Chen, C.T. Ng, J. Lin, Nano Research 4 (2011) 695–704.

[68] X. Zhang, W. Shi, J. Zhu, W. Zhao, J. Ma, S. Mhaisalkar, T.L. Maria, Y. Yang, H. Zhang, H.H. Hng, Nano Research 3 (2010) 643–652.

[69] J.W. Lang, L.B. Kong, W.J. Wu, Y.C. Luo, L. Kang, Chemical Communications (2008) 4213–4215.

[70] X.M. Liu, X.G. Zhang, S.Y. Fu, Materials Research Bulletin 41 (2006) 620–627.

[71] W. Xing, F. Li, Z. Yan, G. Lu, Journal of Power Sources 134 (2004) 324–330.

[72] B. Lu, D. Cao, P. Wang, G. Wang, Y. Gao, International Journal of Hydrogen Energy 36 (2011) 72–78.

[73] C.C. Hu, K.H. Chang, M.C. Lin, Y.T. Wu, Nano Letters 6 (2006) 2690–2695.

[74] T.Y. Wei, C.H. Chen, H.C. Chien, S.Y. Lu, C.C. Hu, Advanced Materials 22 (2010) 347–351.

[75] J. Wang, Y. Song, Z. Li, Q. Liu, J. Zhou, X. Jing, M. Zhang, Z. Jiang, Energy and Fuels 24 (2010) 6463–6467.

[76] F. Meng, Y. Ding, Advanced Materials 23 (2011) 4098–4102.

[77] X. Xia, J. Tu, Y. Zhang, J. Chen, X. Wang, C. Gu, C. Guan, J. Luo, H.J. Fan, Chemistry of Materials 24 (2012) 3793–3799.

[78] V. Tomasic, F. Jovic, Applied Catalysis 311 (2006) 112–121.

[79] G. Centi, S. Perathoner, Catalysis Today 79 (2003) 3–13.

[80] P. Sonstrom, M. Adam, X. Wang, M. Wilhelm, G. Grathwohl, M. Bäumer., Journal of Physical Chemistry C 114 (2010) 14224–14232.

[81] W. Li, Y. Deng, Z. Wu, X. Qian, J. Yang, Y. Wang, D. Gu, F. Zhang, B. Tu, D. Zhao, Journal of the American Chemical Society 133 (2011) 15830–15833.

[82] X. Xie, Y. Li, Z.Q. Liu, M. Haruta, W. Shen, Nature 458 (2009) 746–749.

[83] S.N. Rao, K. Munshi, N. Rao, Journal of Molecular Catalysis A: Chemical 156 (2000) 205–211.

[84] J. Sebastian, K.M. Jinka, R.V. Jasra, Journal of Catalysis 244 (2006) 208–218.

[85] S.K. Pardeshi, R.Y. Pawar, Journal of Molecular Catalysis A: Chemical 334 (2011) 35–43.

[86] Y. Lee, J. Suntivich, K.J. May, E.E. Perry, Y. Shao-Horn, Journal of Physical Chemistry Letters 3 (2012) 399–404.

[87] R. Nakamura, H. Frei, Journal of the American Chemical Society 128 (2006) 10668–10669.

[88] Y.H. Fang, Z.P. Liu, Journal of the American Chemical Society 132 (2010) 18214–18222.
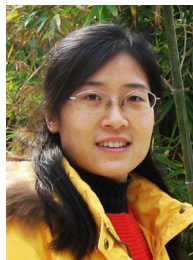
Junfeng Liu received her BS degree and Ph.D. in chemistry from Tsinghua University in 2002 and 2007, respectively. She joined the faculty of State Key Laboratory of Chemical Resource Engineering, Beijing University of Chemical Technology in 2008 as an Associate Professor. Her main research interests focus on controlled synthesis, separation and assembly of monodisperse inorganic nanocrystals, as well as preparation of well-ordered nanostructures and their applications in catalysis, energy and environment

Professor Xiaoming Sun gained his BS and Ph.D. in Department of Chemistry, Tsinghua University in 2000 and 2005, respectively. After postdoctoral work at Stanford University, he joined State Key Laboratory of Chemical Resource Engineering, Beijing University of Chemical Technology at 2008. His main research interests focus on separation and assembly of inorganic nanostructures, synthesis and separation of carbon nanomaterials and their composites, and structure control and opto-/electro-property investigations of oxide nanoarrays.